Original Article

AO SPINE

Global Spine Journal
2023, Vol. 13(8) 2336–2344

DOI: 10.1177/21925682221081797
journals.sagepub.com/home/gsj
Sage

Lumbar Disc Degeneration Affects the Risk of Rod Fracture Following PSO; A Finite Element Study

Ardalan Seyed Vosoughi, MS[1], Niloufar Shekouhi, MS[1], Amin Joukar, MS[1], Michael Zavatsky[2], Vijay K. Goel, PhD[1], and Joseph M. Zavatsky, MD[2]

Abstract

Study Design: Finite element (FE) study.

Objective: Pedicle subtraction osteotomy (PSO) is a surgical method to correct sagittal plane deformities. In this study, we aimed to investigate the biomechanical effects of lumbar disc degeneration on the instrumentation following PSO and assess the effects of using interbody spacers adjacent to the PSO level in a long instrumented spinal construct.

Methods: A spinopelvic model (T10-pelvis) with PSO at the L3 level was used to generate 3 different simplified grades of degenerated lumbar discs (mild (Pfirrmann grade III), moderate (Pfirrmann grade IV), and severe (Pfirrmann grade V)). Instrumentation included eighteen pedicle screws and bilateral primary rods. To investigate the effect of interbody spacers, the model with normal disc height was modified to accommodate 2 interbody spacers adjacent to the PSO level through a lateral approach. For the models, the rods' stress distribution, PSO site force values, and the spine range of motion (ROM) were recorded.

Results: The mildly, moderately, and severely degenerated models indicated approximately 10%, 26%, and 40% decrease in flexion/extension motion, respectively. Supplementing the instrumented spinopelvic PSO model using interbody spacers reduced the ROM by 22%, 21%, 4%, and 11% in flexion, extension, lateral bending, and axial rotation, respectively. The FE results illustrated lower von Mises stress on the rods and higher forces at the PSO site at higher degeneration grades and while using the interbody spacers.

Conclusions: Larger and less degenerated discs adjacent to the PSO site may warrant consideration for interbody cage instrumentation to decrease the risk of rod fracture and PSO site non-union.

Keywords

biomechanics, finite element analysis, pedicle subtraction osteotomy, rod fracture, spine, disc degeneration

Introduction

Sagittal imbalance can be associated with severe back pain and physical disabilities, especially in the elderly population.[1-3] Iatrogenic flatback syndrome, degenerative lumbar flatback deformity, ankylosing spondylitis, post-traumatic kyphosis, and post-laminectomy kyphosis are considered the leading causes of sagittal imbalance.[4-6] Surgical techniques inhibit the deformity progression, achieve spinal balance, and mitigate pain in these patients.[7,8] One of the techniques used to realign and correct the adult spinal deformity is the pedicle subtraction osteotomy (PSO) (with the mean sagittal correction of 25°–

[1]Engineering Center for Orthopedic Research Excellence (E-CORE), Departments of Bioengineering and Orthopaedic Surgery, University of Toledo, Toledo, OH, USA
[2]Spine & Scoliosis Specialists, Tampa, FL, USA

Corresponding Author:
Vijay K. Goel, PhD, Engineering Center for Orthopaedic Research Excellence (E-CORE), Departments of Bioengineering and Orthopaedic Surgery, Colleges of Engineering and Medicine, University of Toledo, 2801 West Bancroft Street, MS 303, NI Hall, Room 5046, Toledo, OH 43606, USA.
Email: Vijay.Goel@utoledo.edu

35° degrees[9]). In this technique, a three-column posterior resection is made, and a V-shaped wedge of the vertebral body is removed through the pedicles. Thus, the wider bone-on-bone contact area provides more stability and decreases the risk of pseudarthrosis. This technique uses the anterior cortex of the vertebral body as a hinge to close the wedge resection. Contoured rod instrumentation is usually utilized to control the closure of the osteotomy.[7] Despite the multiple benefits of the PSO in correcting the sagittal imbalance, it is a technically demanding procedure, and there is a significant risk of serious complications.[10,11] A prevalent complication associated with PSO is post-operative rod breakage reported to be as high as 31.6%.[12,13] Aside from age, pre-operative sagittal imbalance, construct length, the extension of fusion to the pelvis or sacrum, inadequate anterior column support, and rod contouring,[13-18] the lumbar disc geometry has been identified as a risk factor affecting rod failure.[19] The reduction in water and proteoglycan content of the nucleus pulposus (NP) often leads to disc degeneration and loss of disc height.[20-22] Moreover, as degeneration increases, more collagen is secreted in the NP, and hence it becomes stiffer and more fibrotic.[23,24] Therefore, the biochemical and geometrical changes during disc degeneration result in biomechanical alterations of the spinal column, such as changes in stiffness, range of motion (ROM), and loading.

Given the complexity of intervertebral disc (IVD) degeneration biomechanics and the lack of biomechanical assessments of the degenerated spine following PSO, the first purpose of this study was to analyze the effect of lumbar disc degeneration and disc height reduction at 4 different disc grades (healthy; mildly, moderately, and severely degenerated IVDs) on the rods' biomechanics following PSO.

Additionally, investigators have used various surgical techniques to mitigate the mechanical complications and rate of rod fracture following PSO. These include the use of interbody spacers at the disc spaces adjacent to PSO,[12,13,25-27] which improves the stability of the spine and instrumentation, leading to less rod failure. Hence, it is essential to understand the effect of interbody spacers on the rods' biomechanics as well as the ROM and anterior force at the osteotomy site. Thus, our second goal was to investigate, through finite element analysis, the biomechanical effects of interbody spacers (adjacent to the PSO region) in long instrumented fusion constructs.

Materials and Methods

Institutional review board approval and informed consent were not needed for this study. In this study, a previously validated finite element (FE) spinopelvic model (T10-pelvis) with 30° PSO at L3 was used as a basis to produce different grades of disc degeneration models.[28,29] An extensive description of the PSO model development and material properties can be found in the literature.[28,29]

After the PSO was performed, this model was modified to generate 3 different simplified grades of degenerated lumbar discs (mild, moderate, and severe). The degeneration process was performed at all lumbar levels of the spine. To simulate disc degeneration, disc heights were reduced, the compressibility of the nuclei was increased, and the stiffness of the fibers and ligaments was altered. Each disc's height in the lumbar region was reduced based on the grading system of disc degeneration described by Wilke et al.[32] (grades 0, 1, 2, and 3 were corresponding to a 0%, 0–33%, 33–66%, and 66–100% disc height loss). Based on Pfirrmann et al. classification, these grades (healthy, mild, moderate, and severe) correspond to Pfirrmann grade I (normal disc height), Pfirrmann grade III (normal to slightly decreased disc height), Pfirrmann grade IV (normal to moderately decreased disc height), and Pfirrmann grade V (collapsed disc height), respectively.[33-35] In these models, it was assumed that the osteophyte and diffuse sclerosis formation were negligible. The mild, moderate, and severely degenerated disc models were simulated by a 20%, 50%, and 80% reduction in disc heights with respect to their healthy conditions (Figure 1). The anterior, posterior, and average lumbar disc heights (for both healthy and degenerated models with various grades) are presented in Table 1.

As disc degeneration increases, the material properties of nucleus and annulus structures become similar. The Young's modulus of nucleus pulposus was increased from the healthy nucleus material values to the healthy annulus fibrosus ground substance values.[36,37] The nucleus material properties for mild and moderate degenerated discs were linearly interpolated. Based on the literature, the annulus fibrosus ground substance was not affected by disc degeneration (Table 2).[38,39] As disc degeneration increases at a specific lumbar level, fibers and ligaments buckle.[36] Similar to Rohlmann et al.'s study, in our FE models of degenerated discs, to compensate for changes in the length of each ligament and fibers, their non-linear force-deflection curves were offset. Therefore, the buckled ligaments were only activated when they reached their original length.

Models Instrumentation

Design, development and placement of various components of spinal implants, including pedicle screws and rods were extensively discussed in previous publications.[28,29]

Instrumentation included eighteen pedicle screws extending from T10 to the ilium. Pedicles of T10, T11, and T12 vertebral levels were instrumented bilaterally with 4.5 mm × 40 mm pedicle screws. Six 5.5 mm × 45 mm screws were bilaterally anchored at L1, L2, and L4 pedicles. At the L5 and S1 levels, pedicles were instrumented with 6.5 mm x 45 mm and 55 mm screws, respectively. Two 8.5 mm × 80 mm iliac screws were placed such that there was no screw prominence. Two 5.5 mm rods were contoured to fit the pedicle screw tulip heads.

Titanium alloy (Ti6Al4V; E = 115 GPa, υ = .3) and Cobalt-Chromium (CoCr; E = 241 GPa, υ = .3) material properties were adapted from the literature and assigned to pedicle screws and rods, respectively.[40,41] Two connectors were tied to the iliac screw tulip heads and rods to connect them. These connectors were assigned Ti6Al4V material properties.

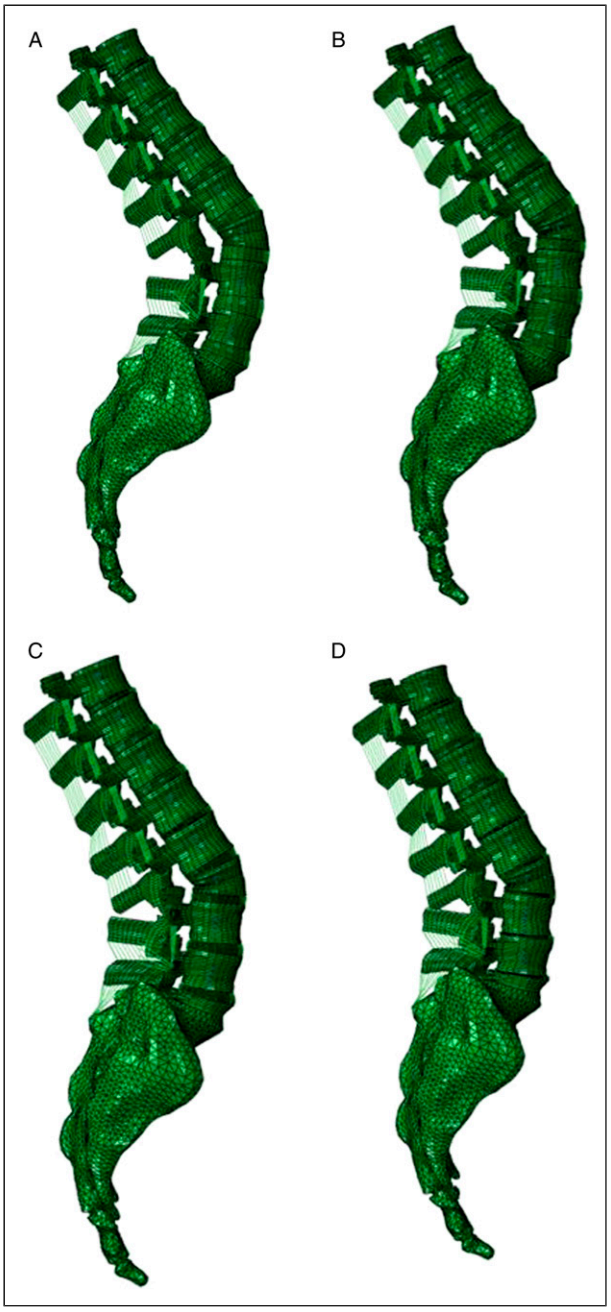

Figure 1. Lateral views of the developed spinopelvic Finite Element models integrated with 30° of Pedicle Subtraction Osteotomy at the L3 level accompanied with various lumbar Intervertebral Disc degeneration grades: (A) healthy discs (normal disc height), (B) mildly degenerated (20% reduction in lumbar disc heights), (C) moderately degenerated (50% reduction in lumbar disc heights), and (D) severely degenerated (80% reduction in lumbar disc heights). For the sake of Intervertebral Discs visualization, the ilium bones were not shown in this figure.

Interbody Spacer FE Models

To investigate the effect of interbody spacers, the aforementioned instrumented PSO model with normal disc heights was modified to accommodate 2 interbody spacers adjacent to the PSO level (Figure 2). A lateral approach was used to instrument the lumbar IVDs with the spacers. For both levels, ideal interbody spacer heights and lordosis angles were calculated from the PSO FE model. Subsequently, the pertaining interbody spacers were meticulously designed in SolidWorks and imported into the Abaqus for model development and analysis.

A total nucleotomy and a partial annulotomy were performed by deleting the corresponding elements of the IVDs. Tie constraints were used to simulate the intervertebral fusions. Interbody spacers were assigned polyether-ether-ketone (PEEK) material properties (E = 3600, v = .4).

Loading and Boundary Conditions

The FE simulation included a two-step analysis: first, to mimic similar kinematics response as those in vivo, follower loads corresponding to the upper body trunk weight in the adult spine were applied to each vertebra.[42] These follower loads were simulated as connector forces with the magnitude of 300 N for the thoracic and 400 N for the lumbar spine. In the second step, pure moments of 7.5 Nm were applied to a reference point, which was kinematically coupled to the superior endplate of the T10 vertebral body in all 3 anatomical directions of flexion (Flex), extension (Ext), lateral bending (LB), and axial rotation (AR). During the entire simulation, the acetabular surfaces of the pelvis were fixed in all degrees of freedom.

To further validate the degenerated lumbar motion segments of L1–L2, L4–L5, and L5–S1, the FE results were compared to the in vitro study of Mimura et al.[43] In their experimental study, they applied a maximum moment of 10 Nm to each motion segment and calculated the corresponding three-dimensional intervertebral motions of each level separately. In our study, a reference point was created and kinematically coupled to the superior endplate of the proximal vertebra. Afterward, a 10 Nm pure moment was applied to this reference point while the inferior endplate of the lower vertebral body was constrained in all degrees of freedom. Due to a lack of data for PSO associated with disc degeneration, we were not able to validate L2–L3 and L3–L4 motion segments.

Data Analysis

The ROM at L1–L2, L4–L5, and L5–S1 segments with different grades of disc degeneration was assessed for validation purposes. The T10-S1 global ROM of all the instrumented spinopelvic models, including normal (with and without interbody spacers) and 3 different grades of IVD degeneration (mild, moderate, and severe), were calculated and compared. For all the models, the stress distribution on the rods was precisely evaluated. The force values acting at the osteotomy sections were recorded following follower load application.

Table 1. Material properties of healthy and degenerated intervertebral discs. Values are adapted from literature.[28,29] The corresponding grades of degeneration are provided based on Pfirrmann Classification.[33-35]

Component/Material	Element formulation	Constitutive model	Material parameters			Pfirrmann classification
			C1	C2	D1	
Nucleus						
Nucleus/Healthy	Hexahedral	Non-linear (Mooney Rivlin)	0.12	0.03	0.0005	Grade I
Nucleus/Mildly degenerated	Hexahedral	Non-linear (Mooney Rivlin)	0.135	0.0338	0.0379	Grade III
Nucleus/Moderately degenerated	Hexahedral	Non-linear (Mooney Rivlin)	0.1575	0.0394	0.0939	Grade IV
Nucleus/Severely degenerated	Hexahedral	Non-linear (Mooney Rivlin)	0.18	0.045	0.15	Grade V
Annulus Fibrosus						
Annulus fibrosus (ground)	Hexahedral	Non-linear (Neo Hookean)	0.348	—	0.3	—
Annulus fibrosus (fiber)	Rebar	Non-linear Hypoelastic	—	—	—	—

Table 2. Maximum von Mises stress values and locations were recorded on the rods in different motions and different grades of IVD degeneration. In models with no spacer, the FE results showed lower von Mises stresses on the rods at higher degeneration grades. Under left bending and left rotation, the critical stress location was observed at the PSO region. Moreover, the rod's critical stresses were reduced by 33% in flexion, compared to models with no spacers.

	No interbody spacers									
	Healthy disc (Pfirrmann grade I)		Mildly degenerated (Pfirrmann grade III)		Moderately degenerated (Pfirrmann grade IV)		Severely degenerated (Pfirrmann grade V)		With interbody spacers	
	Stress value (MPa)	Location	Stress value (%)	Location	Stress value (%)	Location	Stress value (%)	Location	Stress value (%)	Location
FLEX	339	PSO	−5%	PSO	−21%	PSO	−34%	PSO	−33%	L4–L5
EXT	105	L4–L5	−14%	L4–L5	−23%	S1-Iliac screw	−18%	S1-Iliac screw	−4%	L4–L5
LB	221	PSO (right rod)	−3%	PSO (right rod)	−17%	PSO (right rod)	−32%	PSO (right rod)	−11%	L4–L5 (right rod)
RB	221	PSO (left rod)	−9%	PSO (left rod)	−15%	PSO (left rod)	−29%	PSO (left rod)	−9%	L4–L5 (left rod)
LR	256	PSO (right rod)	−6%	PSO (right rod)	−24%	PSO (right rod)	−34%	PSO (right rod)	−13%	L4–L5 (right rod)
RR	256	PSO (left rod)	−11%	PSO (left rod)	−23%	PSO (left rod)	−32%	PSO (left rod)	−14%	L4–L5 (left rod)

FLEX: Flexion, EXT: Extension, LB: Left Bending, RB: Right Bending, LR: Left Rotation, RR: Right Rotation, PSO: Pedicle Subtraction Osteotomy, IVD: Intervertebral Disc.

Results

Model Validation

The FE predictions for L1–L2, L4–L5, and L5–S1 intersegmental rotations, showed similar trends as the in vitro analysis of Mimura et al.[43] Mimura et al. found that with an increase in degeneration's grade, the ROM decreased in flexion/extension and lateral bending[43] while the axial rotation motion initially increased, and decreased in the severely degenerated discs.

Spine's ROM

Within the instrumented models, as degeneration increased, the greatest variation in the T10-S1 ROM was found in flexion/extension. Compared to the instrumented FE model with healthy discs (Pfirrmann grade I), the mildly (Pfirrmann grade III), moderately (Pfirrmann grade IV), and severely (Pfirrmann grade V) degenerated models indicated approximately 10%, 26%, and 40% decrease in flexion/extension motion, respectively. Under lateral bending and axial rotation, different grades of disc degeneration showed similar motions. Under axial rotation, the highest variation in ROM between the healthy (Pfirrmann grade I) and degenerated discs was observed in the model with severe degeneration (Pfirrmann grade V, Figure 3).

Supplementing the instrumented spinopelvic PSO model using interbody spacers reduced the ROM. This reduction was approximately 22%, 21%, 4%, and 11% in flexion, extension, lateral bending, and axial rotation, respectively (Figure 4).

Maximum von Mises Stresses on the Rods

The FE results illustrated lower von Mises stresses on the rods at higher degeneration grades. In degenerated models, the

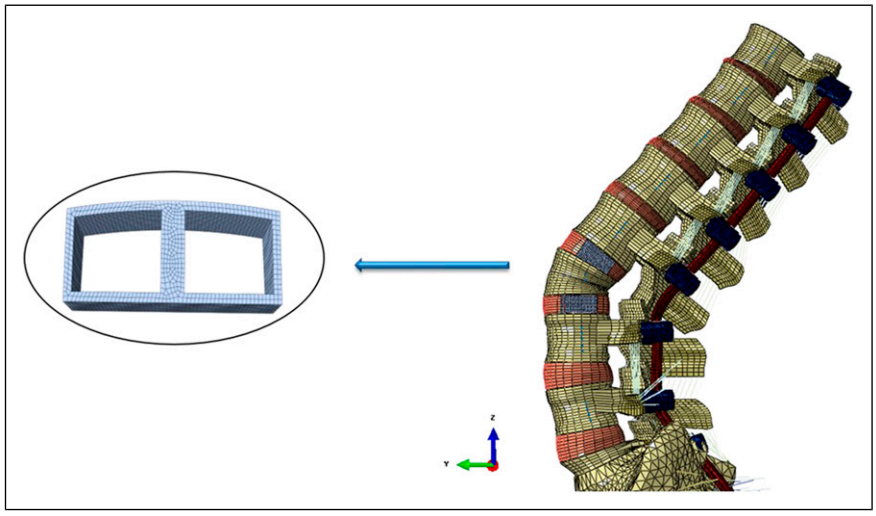

Figure 2. Lateral view of the instrumented spinopelvic model supplemented with interbody spacers adjacent to the Pedicle Subtraction Osteotomy level (L3). On the left side, a top view of the meshed interbody spacer used in the models was demonstrated. For the sake of Intervertebral Discs visualization, the ilium bones were not shown in this figure. A total nucleotomy and a partial annulotomy were performed, and the spacers were implanted through a lateral approach. Tie constraints were used to simulate the intervertebral fusions.

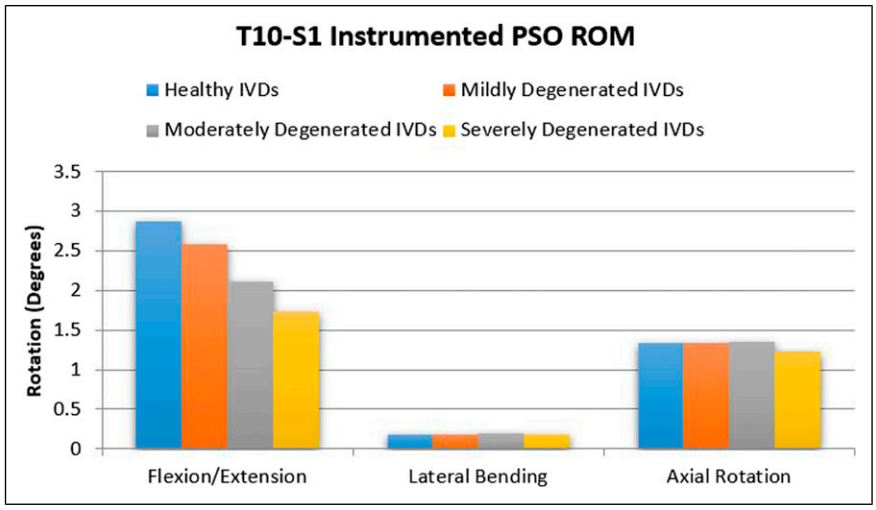

Figure 3. Instrumented T10-S1 global Range of Motion for different loading cases and different grades of disc degeneration in models with no spacer. The highest variation in the T10-S1 Range of Motion was observed in flexion/extension. Moreover, under axial rotation, the highest variation in Range of Motion between the healthy (Pfirrmann grade I) and degenerated discs was observed in the model with severe degeneration (Pfirrmann grade V).

maximum von Mises stress in all the motions (except extension) was recorded at the PSO region. In these models, during the left bending and left rotation motions, the maximum von Mises stress was located at the PSO region of the right rod, and during the right bending and right rotation motions, this value was located at the PSO region on the left rod. Values and locations of the maximum von Mises stress on the rods for various disc degeneration grades in different motions are summarized in Table 2.

Using 2 interbody spacers, 1 above and 1 below the PSO level, had a significant effect in decreasing the maximum von Mises stress on the rods. The FE results indicated the greatest reduction in the maximum von Mises stresses occurred in flexion motion (Table 2). Supplementing the model with 2 interbody spacers reduced the maximum von Mises stress on the rods by 33% in flexion. The least stress reduction was observed in extension motion (approximately by 4%, Table 2). The FE results showed that by adding interbody spacers above and below the PSO level (i.e., L2–L3 and L3–L4), the maximum von Mises stresses shifted the rod's critical stress location from the PSO site at L3, caudally to L4–L5.

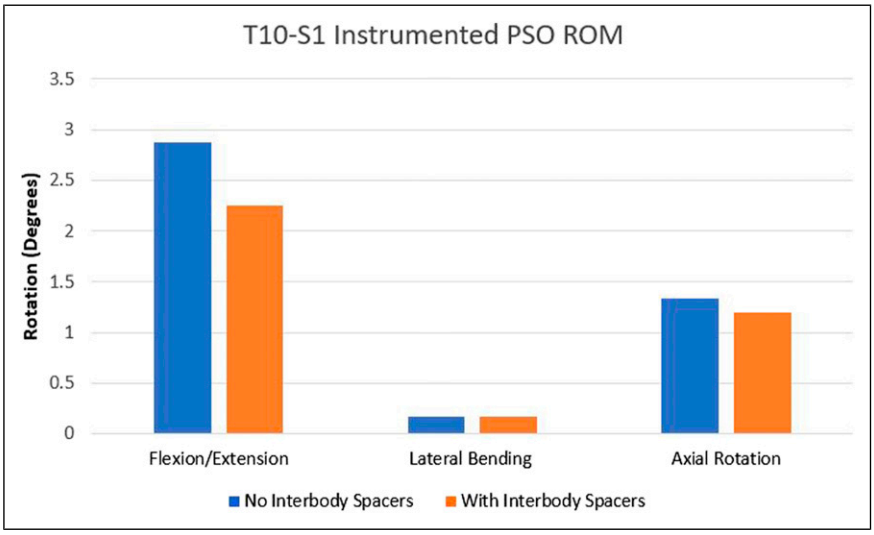

Figure 4. Comparison of the instrumented T10-S1 global Range of Motion for different loading cases with and without interbody spacers. Supplementing the instrumented spinopelvic Pedicle Subtraction Osteotomy model using interbody spacers reduced the T10-S1 Range of Motion by 22%, 21%, 4%, and 11% in flexion, extension, lateral bending, and axial rotation, respectively.

Force at the Osteotomy Region

With increasing disc degeneration, greater forces were observed at the PSO site. Models with healthy (Pfirrmann grade I), mildly (Pfirrmann grade III), moderately (Pfirrmann grade IV), and severely (Pfirrmann grade V) discs degenerated showed 248N, 257.1 N, 272.1 N, and 287.5 N forces at the PSO level, respectively. Furthermore, interbody spacers considerably increased the force magnitude at the PSO site (335.6 N).

Discussion

Pedicle subtraction osteotomy is an intricate surgical intervention to correct sagittal plane deformities. Although PSO is a very effective method to address sagittal malalignment, it is associated with a greater risk of complications. Amongst all complications, rod failure is a major reason for revision surgeries.[9,12,13,45-49] In a multicenter retrospective study, Smith et al. reported 15.8% rod fractures following PSO. In another prospective multicenter investigation, the rate of rod fracture in patients who underwent PSO was reported to be about 22%. To mitigate the mechanical complications and rate of rod fracture following PSO, investigators have used various techniques, including utilizing one or more primary or satellite rods and choosing stiffer CoCr rods that have been demonstrated to be clinically favorable.[25-27] In this regard, a previously published article by Seyed Vosoughi et al.,[28] using a validated PSO model, has shown that adding satellite rods increases the rigidity of the construct and reduces the stress on the primary rods at the PSO level.

In a study by Briski et al.,[19] lumbar disc geometry was recognized as a risk factor affecting rod failure. They reported the patients who experienced rod fracture had larger, non-fused disc heights at the 2 levels immediately cranial and caudal to the PSO level. Unfortunately, there is a lack of experimental work in the literature on degenerated discs and their effects in PSO models. Thus, in an attempt to understand the IVD degeneration biomechanics, 3 different disc degeneration models (mildly, moderately, and severely degenerated) were developed and correlated to the Pfirrmann classification[33-35] in the current study. The simulated healthy, mild, moderate, and severe disc degenerated models are corresponding to Pfirrmann grade I, III, IV, and V, respectively.[33-35] The FE models were validated and analyzed in terms of the spine's ROM, the rod's maximum von Mises stress, and the anterior force across the osteotomy site.

The ROM obtained in this study for models with disc degeneration and at L1–L2, L4–L5, and L5–S1 segments showed similar trends to the in vitro study of Mimura et al.[43] In their cadaver study, with increasing disc degeneration, flexion-extension and lateral bending motions decreased while the axial rotation initially increased then decreased.[43]

Park et al.[50] reported that disc degeneration resulted in reductions in flexion-extension and lateral bending motions, which showed similar ROM trends as our findings for the L4–L5 motion segment. In agreement with previous studies,[43,51] our findings showed that axial rotation increased in the early stages of degeneration and then decreased with severe degeneration.

Our FE results showed that discs with larger height (less degenerated) led to a greater ROM and hence instability at the PSO level. The superior mobility of the segments adjacent to the PSO region resulted in a greater maximum von Mises stress on the rods. Therefore, with increasing degeneration, disc heights decrease, and the stress values on the rods decrease, lowering the risk of rod fracture.

Several studies investigated the location of rod failure following PSO surgery.[17,28,52-54] In a multicenter retrospective study of 443 patients, Smith et al. assessed symptomatic rod fractures following adult spinal deformity correction. Rod fracture was reported at or adjacent to the PSO level in 89% (16 out of 18) of all failures.[10] Tang et al.[52] conducted a biomechanical study on the severity of the rod contour in a PSO setting and found that a rod's fatigue life depends significantly on the severity of the rod angle. Their observation showed a greater risk of fracture in rods with more severe angles. Our results showed that in all grades of disc degeneration, the maximum von Mises stress occurred during flexion motion, during which the stress concentration was observed at the PSO region on the rods. Therefore, the PSO region on the rods is expected to be highly susceptible to failure.

The results further indicated that after follower load application, with an increase in the disc degeneration, a greater amount of load acted across the osteotomy region. Thus, a greater amount of load was carried by the spine's anterior column, and a lower portion of the total load was transferred to the posterior instrumentation, specifically the rods. Therefore, with an increase in disc degeneration, the maximum von Mises stress on the rods is reduced, and thus, rod failure is expected to reduce similarly.

Another goal of this study was to investigate the biomechanical effects of interbody spacers in long instrumented constructs, including a PSO. Enercan et al.[55] suggested using the interbody spacers adjacent to the PSO level to mitigate pseudarthrosis and rod fracture rate. In an in vitro study by Deviren et al.,[56] the use of interbody spacers adjacent to the PSO level was investigated in different loading cases, which showed a modest stabilization effect. Charosky et al.[17] reported a reduction in bending moments on the rods when an interbody spacer was used below the PSO.

In this regard, our computational analyses illustrated that adding interbody spacers above and below the PSO level decreased the rod's maximum von Mises stress by about 33%. Our findings also showed that by adding 2 interbody spacers above and below the PSO level, the ROM in different directions decreased approximately 4–22%. This was in agreement with a biomechanical study of Hallager et al.,[57] which showed a reduction in the rod's strain magnitude under flexion-extension. In another study by Januszewski et al.,[48] adding the interbody spacers reduced the stresses on the rods by 15%, which is consistent with our findings.

Our computational analyses showed that adding the interbody spacers to the PSO construct increased the force acting on the osteotomy region. Adding interbody spacers to the anterior column increased the stiffness of this region, which caused a load transfer to the anterior column. Hence, posterior instrumentation was subjected to a lower force, and consequently, lower chances of rod breakage are expected. This increased the force acting on the PSO region, suggesting lower chances of pseudarthrosis.

Similar to any other finite element analysis, limitations of the current computational study should be taken into account. Spine degeneration is a very complex process, and different factors are involved, which cannot be readily simulated using FE analyses. For instance, due to the complexity of sclerosis and osteophyte formation, and lack of data in the literature on the geometry, material properties, and the rate of development on various IVD levels given various grades of disc degeneration, these were not considered in our models. In addition, the change in discs' height and PSO angles may result in decreased or increased lordosis angles which can affect the instrumentation contours, ROM, and stress values on the rods. In this regard, Tang et al.[52] showed that more severe angles of rod contour have a higher risk of failure. However, the main focus of this article was to analyze the effects of lumbar disc degeneration and disc height reduction on posterior rod stresses following PSO. To accomplish this, all other major variables, including PSO location and angle, sagittal alignment, and instrumentation, were kept constant. Moreover, facets degeneration and annular tears during the degeneration process were neglected in the current simulations. Due to the lack of information for the degenerated annulus material properties, its material properties were not altered within different grades of degeneration. Dynamic analysis of the components such as fatigue test provides a more accurate failure assessment of the rods. No dynamic analysis was simulated in this study. However, fatigue testing of different constructs of this study is suggested for future assessments. Other recommendations for future studies include considering several variables like sclerosis and osteophyte formation on the discs, pre-operative flexibility, pre-operative radiographic parameters (lordosis angle, pelvic incidence, etc.), the extent of fusion levels, weight, PSO correction angle, and size and type of instrumentation.

Conclusion

In the PSO setting, with increasing degeneration, disc heights decrease, resulting in greater amounts of load carried by the anterior column, thus decreasing stress values on the posterior rods and lowering the risk of rod fracture. Adding interbody spacers adjacent to the PSO level reduces the ROM and maximum von Mises stress acting on the posterior rods while enhancing the anterior column stiffness and the force acting on the osteotomy site, thus decreasing the risk of PSO pseudarthrosis. Interbody cage instrumentation above and below the PSO site in selected patients may reduce the risk of posterior rod failure and PSO pseudarthrosis.

Declaration of Conflicting Interests

The author(s) declared no potential conflicts of interest with respect to the research, authorship, and/or publication of this article.

Funding

The author(s) disclosed receipt of the following financial support for the research, authorship, and/or publication of this article: This study

was supported partly by National Science Foundation (NSF) IIP-136197 Industry/University Cooperative Research Center at the University of California, San Francisco, CA, Ohio State University (OSU), Columbus, OH, and The University of Toledo, Toledo, OH (www.nsfcdmi.org)

ORCID iDs

Ardalan Seyed Vosoughi https://orcid.org/0000-0002-5820-8942
Amin Joukar https://orcid.org/0000-0003-2647-7432
Vijay K. Goel https://orcid.org/0000-0002-9175-5366

References

1. Deviren V, Youssef J, Orndorff D, et al. Current status of adult spinal deformity; 2013.
2. Yamato Y, Hasegawa T, Kobayashi S,et al. Calculation of the target lumbar lordosis angle for restoring an optimal pelvic tilt in elderly patients with adult spinal deformity. *Spine*. 2016; 41(4):E211-E217.
3. Kiapour A, Joukar A, Elgafy H, Erbulut DU, Agarwal AK, Goel VK. Biomechanics of the sacroiliac joint: anatomy, function, biomechanics, sexual dimorphism, and causes of pain. *Int J Spine Surg*. 2020;14(s1):3-13.
4. Booth KC, Bridwell KH, Lenke LG, Baldus CR, Blanke KM. Complications and predictive factors for the successful treatment of flatback deformity (fixed sagittal imbalance). *Spine*. 1999;24(16):1712-1720.
5. Casey MP, Asher MA, Jacobs RR, Orrick JM. The effect of Harrington rod contouring on lumbar lordosis. *Spine*. 1987; 12(8):750-753.
6. Joseph SA Jr, Moreno AP, Brandoff J, Casden AC, Kuflik P, Neuwirth MG. Sagittal plane deformity in the adult patient. *J Am Acad Orthop Surg*. 2009;17(6):378-388.
7. Kose KC, Bozduman O, Yenigul AE, Igrek S. Spinal osteotomies: indications, limits and pitfalls. *EFORT Open Rev*. 2017; 2(3):73-82.
8. Joukar A, Kiapour A, Elgafy H, Erbulut DU, Agarwal AK, Goel VK. Biomechanics of the sacroiliac joint: surgical treatments. *Int J Spine Surg*. 2020;14(3):355-367.
9. Schwab F, Blondel B, Chay E, et al. The comprehensive anatomical spinal osteotomy classification. *Neurosurgery*. 2015; 76(Suppl 1):S33-S41.
10. Smith JS, Sansur CA, Donaldson WF III, et al. Short-term morbidity and mortality associated with correction of thoracolumbar fixed sagittal plane deformity: a report from the scoliosis research society morbidity and mortality committee. *Spine*. 2011;36(12):958-964.
11. Charles YP, Yu B, Steib JP. Sacroiliac joint luxation after pedicle subtraction osteotomy: report of two cases and analysis of failure mechanism. *Eur Spine J*. 2016;25(1):63-74.
12. Smith JS, Shaffrey E, Klineberg E, et al. Prospective multicenter assessment of risk factors for rod fracture following surgery for adult spinal deformity. *J Neurosurg Spine*. 2014; 21(6):994-1003.
13. Smith JS, Shaffrey CI, Ames CP, et al. Assessment of symptomatic rod fracture after posterior instrumented fusion for adult spinal deformity. *Neurosurgery*. 2012;71(4):862-867.
14. Barton C, Noshchenko A, Patel V, Cain C, Kleck C, Burger E. Risk factors for rod fracture after posterior correction of adult spinal deformity with osteotomy: a retrospective case-series. *Scoliosis*. 2015;10(1):30.
15. Berjano P, Bassani R, Casero G, Sinigaglia A, Cecchinato R, Lamartina C. Failures and revisions in surgery for sagittal imbalance: analysis of factors influencing failure. *Eur Spine J*. 2013;22(6):S853-S858.
16. Luca A, Ottardi C, Sasso M, et al. Instrumentation failure following pedicle subtraction osteotomy: the role of rod material, diameter, and multi-rod constructs. *Eur Spine J*. 2017;26(3):764-770.
17. Charosky S, Moreno P, Maxy P. Instability and instrumentation failures after a PSO: a finite element analysis. *Eur Spine J*. 2014; 23(11):2340-2349.
18. Joukar A, Mehta J, Marks D, Goel VK. Lumbar-sacral destruction fixation biomechanics: a finite element study. *Spine J*. 2017;17(11):S335.
19. Briski D, Zavatsky J, Cook B. How lumbar disc geometrics affect the risk for rod fracture in patients undergoing adult spinal deformity surgery: an initial report. *Global Spine J*. 2016;6(1_suppl l):1612-1624.
20. Kalb S, Martirosyan NL, Kalani MY, Broc GG, Theodore N. Genetics of the degenerated intervertebral disc. *World Neurosurg*. 2012;77(3-4):491-501.
21. Benneker LM, Heini PF, Anderson SE, Alini M, Ito K. Correlation of radiographic and MRI parameters to morphological and biochemical assessment of intervertebral disc degeneration. *Eur Spine J*. 2005;14(1):27-35.
22. Urban JP, McMullin JF. Swelling pressure of the lumbar intervertebral discs: influence of age, spinal level, composition, and degeneration. *Spine*. 1988;13(2):179-187.
23. Frobin W, Brinckmann P, Kramer M, Hartwig E. Height of lumbar discs measured from radiographs compared with degeneration and height classified from MR images. *Eur Radiol*. 2001;11(2):263-269.
24. Inoue N, Espinoza Orías AA. Biomechanics of intervertebral disk degeneration. *Orthop Clin N Am*. 2011;42(4):487-vii.
25. Barrey C, Perrin G, Michel F, Vital JM, Obeid I. Pedicle subtraction osteotomy in the lumbar spine: indications, technical aspects, results and complications. *Eur J Orthop Surg Traumatol*. 2014;24(1):S21-S30.
26. Cho KJ, Kim KT, Kim WJ, et al. Pedicle subtraction osteotomy in elderly patients with degenerative sagittal imbalance. *Spine*. 2013;38(24):E1561-E1566.
27. Hyun SJ, Lenke LG, Kim YC, Koester LA, Blanke KM. Comparison of standard 2-rod constructs to multiple-rod constructs for fixation across 3-column spinal osteotomies. *Spine*. 2014;39(22):1899-1904.
28. Vosoughi AS, Joukar A, Kiapour A, et al. Optimal satellite rod constructs to mitigate rod failure following pedicle subtraction osteotomy (PSO): a finite element study. *Spine J*. 2019;19(5):931-941.

29. Seyed Vosoughi A. *Mitigating the Biomechanical Complications Following Pedicle Subtraction Osteotomy: A Finite Element Analysis*. University of Toledo; 2017.
30. Ottardi C, Galbusera F, Luca A, et al. Finite element analysis of the lumbar destabilization following pedicle subtraction osteotomy. *Med Eng Phys*. 2016;38(5):506-509. doi:10.1016/j.medengphy.2016.02.002.
31. Goffin JM, Pankaj P, Simpson AH. A computational study on the effect of fracture intrusion distance in three-and four-part trochanteric fractures treated with Gamma nail and sliding hip screw. *J Orthop Res*. 2014;32(1):39-45.
32. Wilke HJ, Rohlmann F, Neidlinger-Wilke C, Werner K, Claes L, Kettler A. Validity and interobserver agreement of a new radiographic grading system for intervertebral disc degeneration: part I. Lumbar spine. *Eur Spine J*. 2006;15(6):720-730.
33. Pfirrmann CW, Metzdorf A, Zanetti M, Hodler J, Boos N. Magnetic resonance classification of lumbar intervertebral disc degeneration. *Spine*. 2001;26(17):1873-1878.
34. Griffith JF, Wang YX, Antonio GE, et al. Modified Pfirrmann grading system for lumbar intervertebral disc degeneration. *Spine*. 2007;32(24):E708-E712.
35. Urrutia J, Besa P, Campos M, et al. The Pfirrmann classification of lumbar intervertebral disc degeneration: an independent inter- and intra-observer agreement assessment. *Eur Spine J*. 2016;25(9):2728-2733.
36. Krismer M, Haid C, Behensky H, Kapfinger P, Landauer F, Rachbauer F. Motion in lumbar functional spine units during side bending and axial rotation moments depending on the degree of degeneration. *Spine*. 2000;25(16):2020-2027.
37. Rohlmann A, Zander T, Schmidt H, Wilke HJ, Bergmann G. Analysis of the influence of disc degeneration on the mechanical behaviour of a lumbar motion segment using the finite element method. *J Biomech*. 2006;39(13):2484-2490.
38. Elliott DM, Setton LA. Anisotropic and inhomogeneous tensile behavior of the human anulus fibrosus: experimental measurement and material model predictions. *J Biomech Eng*. 2001;123(3):256-263.
39. Skaggs DL, Weidenbaum M, Iatridis JC, Ratcliffe A, Mow VC. Regional variation in tensile properties and biochemical composition of the human lumbar anulus fibrosus. *Spine*. 1994;19(12):1310-1319.
40. Kiapour A. *Investigation Into Lumbar Spine Biomechanics of 360 Motion Preservation Systems*. The University of Toledo; 2010.
41. Joukar A, Chande RD, Carpenter RD, et al. Effects on hip stress following sacroiliac joint fixation: a finite element study. *JOR spine*. 2019;2(4):e1067.
42. Frankel B, Semler ME, Walker C, Fedorov S. *Percutaneous Modular Head-to-Head Cross Connector*. Google Patents; 2015.
43. Mimura M, Panjabi MM, Oxland TR, Crisco JJ, Yamamoto I, Vasavada A. Disc degeneration affects the multidirectional flexibility of the lumbar spine. *Spine*. 1994;19(12):1371-1380.
44. Campana S, de Guise JA, Rillardon L, Mitton D, Skalli W. Lumbar intervertebral disc mobility: effect of disc degradation and of geometry. *Eur J Orthop Surg Traumatol*. 2007;17(6):533-541.
45. Wang MY, Bordon G. Mini-open pedicle subtraction osteotomy as a treatment for severe adult spinal deformities: case series with initial clinical and radiographic outcomes. *J Neurosurg Spine*. 2016;24(5):769-776.
46. Upadhyaya CD, Berven S, Mumaneni PV. Spondylolisthesis following a pedicle subtraction osteotomy: case report. *Neurosurg Focus*. 2010;28(3):E16.
47. La Barbera L, Wilke HJ, Liebsch C, et al. Biomechanical in vitro comparison between anterior column realignment and pedicle subtraction osteotomy for severe sagittal imbalance correction. *Eur Spine J*. 2020;29(1):36-44.
48. Januszewski J, Beckman JM, Harris JE, Turner AW, Yen CP, Uribe JS. Biomechanical study of rod stress after pedicle subtraction osteotomy versus anterior column reconstruction: a finite element study. *Surg Neurol Int*. 2017;8:207.
49. Benoit D, Wang X, Crandall DG, Aubin CÉ. Biomechanical analysis of sagittal correction parameters for surgical instrumentation with pedicle subtraction osteotomy in adult spinal deformity. *Clin Biomech*. 2020;71:45-52.
50. Park WM, Kim YH, Lee S. Effect of intervertebral disc degeneration on biomechanical behaviors of a lumbar motion segment under physiological loading conditions. *J Mech Sci Technol*. 2013;27(2):483-489.
51. Schmidt H, Kettler A, Rohlmann A, Claes L, Wilke HJ. The risk of disc prolapses with complex loading in different degrees of disc degeneration–a finite element analysis. *Clin Biomech*. 2007;22(9):988-998.
52. Tang JA, Leasure JM, Smith JS, Buckley JM, Kondrashov D, Ames CP. Effect of severity of rod contour on posterior rod failure in the setting of lumbar pedicle subtraction osteotomy (PSO) a biomechanical study. *Neurosurgery*. 2013;72(2):276-283.
53. Patwardhan AG, Havey RM, Carandang G, et al. Effect of compressive follower preload on the flexion–extension response of the human lumbar spine. *J Orthop Res*. 2003;21(3):540-546.
54. Cho SK, Bridwell KH, Lenke LG, et al. Major complications in revision adult deformity surgery: risk factors and clinical outcomes with 2-to 7-year follow-up. *Spine*. 2012;37(6):489-500.
55. Enercan M, Ozturk C, Kahraman S, Sarıer M, Hamzaoglu A, Alanay A. Osteotomies/spinal column resections in adult deformity. *Eur Spine J*. 2013;22(2):S254-S264.
56. Deviren V, Tang JA, Scheer JK, et al. Construct rigidity after fatigue loading in pedicle subtraction osteotomy with or without adjacent interbody structural cages. *Global Spine J*. 2012;2(4):213-220.
57. Hallager DW, Gehrchen M, Dahl B, et al. Use of supplemental short pre-contoured accessory rods and cobalt chrome alloy posterior rods reduces primary rod strain and range of motion across the pedicle subtraction osteotomy level: an: in vitro: biomechanical study. *Spine*. 2016;41(7):E388-E395.